Size Control of InP Nanowires by *in-situ* annealing and Its Application to the Formation of InAsP Quantum Dots

Masahiro Sasaki, Tomoya Akamatsu, Katsuhiro Tomioka, and Junichi Motohisa

Graduate School of Information Science and Technology and Research Center for Integrated Quantum Electronics, Hokkaido University, North 14, West 9, Sapporo 060-0814, Japan

E-mail: motohisa@ist.hokudai.ac.jp

August 2023

Abstract. We carried out *in-situ* annealing of InP Nanowires (NWs) in a metal-organic vapor phase epitaxial (MOVPE) growth reactor to control and reduce the tip size of InP NWs. InP NWs were grown by selective-area (SA) MOVPE on partially masked (111)A InP substrates, and annealing was successively applied in tertiarybutylphosphine (TBP) ambient. Initially, the InP NWs had a hexagonal cross-section with $\{11\bar{2}\}$ facets vertical to the substrates; they became tapered, and the edges were rounded by annealing. By appropriately selecting the annealing temperature and initial NW diameter, the tip size of the NW was reduced and NWs with a tip size of 20nm were successfully formed. Subsequently, a thin InAsP layer was grown on the annealed NWs and their photoluminescence was investigated at low temperatures. The characterization results indicated the formation of InAsP quantum dots (QDs) emitting in the telecom band. Our approach is useful for reducing the size of the NWs and for the controlled formation of InAsP QDs embedded in InP NWs in photonic devices compatible with telecom bands.

1. Introduction

Semiconductor nanowires (NWs) formed using bottom-up crystal growth techniques have attracted considerable interest because of their unique properties and potential for various applications in electronic [1–4] and photonic devices [5–7], and quantum information processing [8, 9]. In particular, InP-based heterostructured NWs are promising for photonic devices, because they have a direct band gap compatible with the telecom band [10, 11]. NW devices operating in telecom bands, such as light-emitting diodes [12, 13] and lasers [14] have been fabricated using InAsP/InP heterostructures in NWs.

The size and shape of NWs significantly influence their electronic and optical properties, such as quantum confinement [15], emission properties [16–19], and lasing

properties [20–22], and so on. Regarding the lateral quantum confinement for realizing a one-dimensional electron system, the required diameter of the NWs should be less than 20 nm for InP-based NWs as well as GaAs-based NWs [15]. These requirements hold for three-dimensional quantum-confined structures, namely, quantum dots (QDs) in NWs (NW-QDs). Thus, if QDs can be formed at the tips of the NWs, the tip diameter of the NWs should be 20 nm or less. One application of NW-QD is as single [19] and entangled photon emitters [23,24] and it is important to achieve strong lateral quantum confinement for reproducible and stable emission from QDs.

The control of the lateral size of NWs and their limitations are dependent on the NW growth method. For NWs formed via a catalysis-assisted mechanism, the size of the catalyst determines the diameter of the NWs. Some early studies reported successful formation and diameter control in III-V NWS less than 20 nm via catalysis-assisted solution or vapor-liquid-solid (VLS) growth [25,26]. However, very few studies [10,11] have succeeded in forming thin NWs based on epitaxial growth using molecular beam epitaxy (MBE) and metal-organic vapor-phase epitaxy (MOVPE), although these are much more suitable and demanded approaches for device applications. This is presumably due to the difficulty in controlling the size of the catalyst in the epitaxial growth. In the case of selective-area growth [27–29], the size of the mask hole is the most critical factor for determining the NW diameter. As an example, we demonstrated InGaAs NWs with diameters smaller than 40 nm starting with a mask hole size of 30 nm [30]. However, the larger diameter of the grown NWs than the mask opening indicates the existence of lateral growth on the NW sidewalls, namely, the coexistence of vertical and axial growth, which some difficulty in accurate control including other structural parameters of the NW, such as the pitch of the NW array, and the NW length. Indeed, we introduced a two-step growth method to independently control the density and size of NWs in [30], and a more systematic study is required to further reduce the NW size. The only successful realization of InP NWs and InAsP quantum dots with lateral sizes of less than 20 nm was demonstrated by Dalacu *et al.* using a combination of VLS growth and selective-area growth [19,31].

An alternative method to control the diameter of NWs is reverse-reaction growth or thermal decomposition/etching via post-growth treatment. This was reported for GaN NWs in Ref. [32] and for MBE-grown GaAs [15,33,34] and InAs NWs [35]. Using this method, the lateral quantum confinement and its variation with NW size were successfully confirmed. On the other hand, control of the size by post-growth thermal treatment has been less attempted [36] for InP-based NWs with their technological importance as described above. One of the difficulties in the post-growth treatment of InP is its low congruent evaporation temperature, which is much lower than that of GaAs [37]. Therefore, more careful and accurate control of the annealing conditions is required to avoid excess evaporation.

In this study, we attempted the *in-situ* thermal annealing of InP NWs in a MOVPE system to control their size. We observed that the NWs were tapered and rounded after the annealing. This is a result of the mass transport of In from the edges of the

sidewalls to the tips of the NWs. Depending on the annealing temperature and initial NW diameter, diffused In contributes to axial growth or evaporation. Tapering and axial growth on the tip induced size reduction at the tip of the NW. As an application of this method, we present the results of the growth of InAsP/InP heterostructures on annealed NWs and demonstrate the formation of InAsP QDs in NWs. While the formation of QDs in NWs and their optical properties have been reported in many literature [16–19,23,31,36,38–46], reports on the sharp emission originating from three-dimensional quantum confinement are limited. In particular, few studies have reported on the emission of excitons and biexcitons in the telecom C-band ($1.53 \sim 1.565$ μm) of QDs formed in NWs. In the present study, we confirmed exciton and biexciton emissions in the C-band from a single InAsP QD formed in a single InP NW.

2. Experimental Procedure

InP NWs were grown by SA-MOVPE on partially masked InP (111)A substrates using trymethylindimum (TMIn), tertiarybutylphosphine (TBP), and AsH_3 as source materials. After the deposition of an 18 nm-thick SiO_2 mask on the InP (111)A substrates, SiO_2 was partially removed using electron beam (EB) lithography, reactive ion etching (RIE), and wet chemical etching to form circular openings (diameter d_0) in the mask. The mask opening was arranged to form a triangular array with constant pitch a of 1 μm, and we investigated an NW array with d_0 =110 or 180 nm. SA-MOVPE of the InP NWs was carried out in a low-pressure MOVPE system at a growth temperature of 660 °C for 21 min. The partial pressure of TMIn ([TMIn]) and TBP ([TBP]) were 2.74×10^{-6} and 4.05×10^{-5} atm, respectively. The resultant V/III ratio was 14.8. This relatively high temperature and low V/III ratio are our standard conditions for the growth of wurtzite InP NWs [27]. After NW growth, *in-situ* annealing in the MOVPE reactor was carried out in TBP ambient with $[\mathrm{TBP}] = 3.24 \times 10^{-4}$ atm. The annealing temperature T_A were 600, 630, and 660 °C. The annealing times t_A were set to 5, 10, and 20 min.

The growth of InP/InAsP/InP heterostructured NWs were performed after annealing the InP NWs to form NW-QDs. InAsP was grown at 580 °C for 3 sec with $[\mathrm{TMIn}] = 9.89 \times 10^{-7}$ atm, followed by the InP growth for capping at 580 °C and 660 °C for 2 and 10 min with $[\mathrm{TMIn}] = 2.74\times10^{-6}$ and $[\mathrm{TBP}] = 1.62\times10^{-4}$ atm. The ratio $p_{\mathrm{AsH_3}} = [\mathrm{AsH_3}]/([\mathrm{AsH_3}]+[\mathrm{TBP}])$, where $[\mathrm{AsH_3}]$ is the partial pressure of AsH_3, and the partial pressure of AsH_3 in group V sources during InAsP growth was set to 54 %.

3. Effects of Annealing on InP NW

3.1. Dependence on Annealing Temperature

Figures 1 and 2 summarize the results of annealing and its temperature dependence for different NW diameters d before annealing. The annealing time t_A was 10 min. The diameters d of the starting NWs were 240 nm and 120 nm in Figures 1 and 2, respectively.

They were formed from masks with opening diameters d_0 of 180 and 110 nm. The initial shape of the NWs was hexagonal pillars surrounded by $\{11\bar{2}\}$ facets vertical to the (111)A substrates, as shown in Figures 1(a) and 2(a). Specifically, the grown InP NWs had a wurtzite crystal structure, as expected from the growth conditions [27], and the sidewall facet was equivalent to $\{1\bar{1}00\}$ plane of the wurtzite crystal.

It can be seen that all NWs became tapered and the edges of the hexagons were rounded after annealing. This indicated the detachment of In and P from the edges of the hexagon. In addition, the change in the shape and height depends on the annealing temperature T_A and d. For d = 240 nm and $T_A > 630$°C, one can see that thinner and shorter sections were formed at the tip of the NW. We believe that this is the result of self-catalyzed VLS growth that occurs during annealing. On the other hand, different behaviors were observed for NWs with d = 120 nm. That is, at T_A = 630 °C and 660 °C, the height of the NW became extremely low. The average height for NW with d =120 nm was 838 nm before annealing, and they became 89.8 and 88.7 nm after annealing at 630 and 660 °C, respectively. This shows the thermal evaporation of In and P. Furthermore, thin and short sections were formed at the tips of the NWs for T_A = 630 °C and 660 °C with d =120 nm. They are also thought to be formed by self-catalyzed VLS growth during annealing.

To discuss the change in the shape and height more quantitatively, we measured the top size of the NWs and calculated their volume before and after annealing. The results are shown in Figure 3. Here, the average top size d_t obtained from 10 to 30 NWs is shown for each sample, and it is assumed that the NWs have a circular or hexagonal conical shape for annealed NWs for the calculation of the volume. Thinner sections at the top of NWs, as shown in Figures 1(c) and (d), are also considered. We can see that the top size of the NWs was reduced by annealing for both d = 240 and 120 nm and the reduction of the volume and its temperature dependence is clear for NWs with d = 120 nm. For NWs with d = 240 nm, the volumes decreased considerably at 630 °C and increased again at 660 °C. While more volume reduction is naturally expected at higher temperatures, we confirmed that the results at 660 °C was reproducible. Therefore, we think it reasonable that the volume change is not very large for NWs with d = 240 nm in the investigated temperature range. This small reduction in the volume of NWs with d = 240 nm obtained at T_A = 660°C is attributed to the formation of thin and short sections at the top of the NWs, suggesting mass transport of In from the sidewall to the top and axial growth of the short sections.

3.2. Dependence on annealing time

Next, we investigated the dependence on the annealing time, t_A at T_A = 600 °C. t_A was varied from 5 to 20 min. The results are summarized in Figure 4 (see Supplementary Information for the SEM images). In Fig. 4(a), the bottom d_b and top d_t diameter of the NWs are plotted as a function of t_A. The difference between d_b and d_t increased with t_A, but there were no systematic changes in diameter. The measurement of the

volume also confirmed the absence of a systematic change in volume with t_A for both d = 120 and 240 nm NWs. Thus, within the experimental error, it is concluded that the volumes are almost constant and independent of t_A. This change in the shape without a change in the volume suggests that the evaporation of In was very small and was not the main reason for the change in the size at 600 °C. On the other hand, Figure 4(c) shows that the difference in the top d_t and bottom size d_b of the NW became larger with t_A. The results also showed that the difference between d_b and d_t was larger for a set of NW with d = 120 nm. Furthermore, when we plotted $\Delta d = d_b - d_t$ as a function of NW height for t_A = 5 min, the higher NWs with d= 120 nm had larger Δd, as shown in Figure 4(c). The results also show that the tapered angle is almost constant for NWs with d = 120 nm, and is larger for samples with d = 120 nm as compared with d= 240 nm. Therefore, we concluded that In detached from the sidewalls diffused to the top of the NWs and crystallized at the top and that d_t became smaller for smaller d_b, suggesting that thinner NWs are easier to be thinned by annealing. The tapered angle seems to be less constant for d= 240 nm NWs, but the dependence of the tapered angle on NW diameter and its reasons are not clear at present.

3.3. Mechanism of shape change during annealing

The experimental results described above confirm that the tip size of the InP NWs was reduced by annealing. They also showed that the cross-sectional shape of NW changed from hexagonal to rounded. Furthermore, the NWs were tapered. If we look at the experimental results in Figures 1–4 in more detail, the results of annealing can be classified into cases with significant volume reduction and those with relatively little volume change. The former was observed at d = 120 nm, T_A = 630 °C and 660 °C (Figure 2(c) and (d)). In these cases, In evaporated because of the high annealing temperature. In contrast, in the latter case, the decrease in NW height was small and even increased in some cases. Therefore, the change in the shape of the InP NWs was first induced by the decomposition of InP and the desorption of P at the edge of the hexagon on the sidewalls of the NWs. Most of the remaining In did not immediately desorb, but caused mass transport from the sidewalls to the top. Then, diffused In reacted with the P precursor in the gas phase and contributed to the vertical growth of NWs unless the annealing temperature was too high. Furthermore, when the growth proceeded at the top, In droplets were formed and the growth took place by the self-catalyzed VLS mechanism, as shown in Figures 1(c) and 1(d) (and in Figure 2(d)). It is also likely that the growth proceeded in the [111]A direction by the normal epitaxial growth mode without depending on the droplets, as shown in Figures 1(b) and 2(b). Priante *et al.* [47] reported the stop and restart of self-catalyzed GaAs NW growth by the consumption and recreation of Ga droplets at the top of NWs. Our present results for VLS growth are very similar to theirs in the sense that catalysts can be created intentionally in the growth chamber or reactor and be used to tailor the size of the NWs. Thus, the results demonstrated the possibility of realizing thin NWs by

controlling the droplet size, as reported by Kim *et al.* [48].

The experimental results also show that these desorption and growth modes depend not only on the annealing temperature T_A but also on the NW diameter d before annealing. This can be explained as follows; when T_A was low, the amount of P desorbed from the sidewall of the NW was small, so the amount of In diffused from the sidewall was also small. When the amount of In near the top was sufficiently smaller than the amount of P precursor in the atmosphere, normal epitaxial growth contributed to the axial growth of the NWs. However, as the annealing temperature increased, the amount of P desorbed from the sidewalls increased; thus, the amount of In diffusing from the sidewalls to the top also increased. Consequently, the amount of In near the top is greater than the number of P precursors in the surrounding atmosphere, forming In droplets. If the NW diameter is sufficiently large, self-catalyzed VLS growth forms a thin section at the tip. However, when the diameter of the NW was small, the In droplets were small and the In droplets easily evaporated, resulting in the desorption of not only P but also In, leading to a decrease in volume. The shape change of the NWs by annealing describe here is summarized in Figure 5.

In reality, the appearance of two different shape changes, and the appearance of two types of growth modes are thought to exhibit continuous transition depending on the annealing conditions and the size parameters of the NWs. However, this appeared to be abrupt. We also have to admit that the explanation presented in the previous paragraph contains some contradiction: as we describe in the next section, VLS growth occurred in thinner NW, as shown in Figure 6. We speculate that a consistent explanation is possible if the thermal stability of NWs is very sensitive to their diameter and if the In evaporation rate changes significantly with temperature. That is, if the change in the decomposition rate of InP is significantly higher for smaller NWs, the mass transport of In from the sidewall to the top increases significantly, leading to the formation of In droplets at the thin NW tip. The dependence of the thermal stability on the NW size would be plausible if one considered the cross-sectional shape of the NWs after annealing, where they were closer to the hexagon for NWs with $d = 240$ nm but were more rounded and almost circular for those with $d = 120$ nm, as shown in Figures 1 and 2. It is also possible that the decomposition is accelerated in thinner NWs because the decomposition of flat facet sidewalls is slower than that of rough sidewalls, as demonstrated in Ref. [34]. In general, the In atom density at the top of the NW during annealing depends on the number of In atoms that decompose and diffuse from the sidewalls, number of In atoms that are recrystallized and incorporated into the NW, and the amount of In atoms that evaporate. Depending on the balance between the supply and consumption rate of In, there are cases in which growth proceeds with and without In droplets and cases in which In desorption is dominant. A more accurate evaluation of each quantity and its temperature and NW size dependence are necessary for a more quantitative discussion, which is beyond the scope of this study.

3.4. Formation of thin NWs

The above experimental results suggest that annealing at a temperature of 600 °C is more appropriate for reducing the lateral NW size. As shown in Figure 4(c), it is also considered that the smaller the initial NW size, the more effectively the NW can be miniaturized. Based on this idea, we applied *in-situ* annealing to InP NWs at 600 °C. Figure 6 shows the results obtained for NWs grown in a pattern with an opening diameter of $d_0 = 60$ nm. The annealing time was 5 minutes. Although the NW dimension d before growth was not measured precisely, a very thin InP NW was formed on top with a cross-sectional dimension of approximately 20 nm at the tip as expected. As there was a clear size difference between the wide bottom part and the narrow top part in this NW array, it is thought that the top part was grown by the VLS mechanism. The growth of the VLS mechanism can be explained by the thermal instability of thin NWs.

4. Formation of InAsP QD

Finally, NW-QDs were formed by growing InAsP and InP after thermal annealing of the InP NWs, and low-temperature micro-photoluminescence (PL) characterization was performed. To form and evaluate a single and small QD in the NWs, we measured the NWs obtained from a masked substrate with an opening diameter d_0 of 60 nm and a pattern pitch a of 3 μm. A typical SEM image of a NW-QD is shown in Figure 7(a). The diameter of the NW was greater than the opening diameter d_0, and the expected tip size of the annealed InP NWs. This was attributed to the lateral growth of InP under low-temperature and high V/III ratio growth conditions after the growth of InAsP, as schematically shown in Figure 7(b). We believe that In droplets were consumed by InP NW growth or vapor-solid growth occured in InP, and that the QDs were formed without In droplets, similar to the case reported in Ref. [45]. Figure 7(c) shows the PL spectrum of the single NW-QDs under an excitation intensity I of 109 W/cm^2 measured at 4 K. Multiple peaks including sharp lines were observed. Emissions above 1.43 eV were originated from InP. Broad and emissions with multiple peaks in the energy range from 0.9 to 1.4 eV were attributed to the emission from the InAsP layer, which presumably formed in the sidewall of tapered NWs, as shown in Figure 7(b). In addition, very narrow peaks were observed at approximately 0.8 eV. Figure 7(d) shows their excitation intensity dependence. We here focus on two peaks labelled X and XX, which were respectively confirmed above I of 1.06 and 17.7 W/cm^2. At each I, the peak X was located at 0.793 eV (1.563 μm) and had a linewidth of 2.24 meV (obtained by Gaussian fitting), and peak XX was located at 0.798 eV (1.553 μm) and had a linewidth of 0.855 meV. Figure 7 (e) shows the integrated intensity of the two peaks X and XX and their dependence on I, plotted on a logarithmic scale. The results indicated that the integrated intensity of peaks X and XX were proportional to linear and quadratic dependence on I, respectively, when I was sufficiently low. These were very similar to

our previous results reported in Refs. [49–51]. The peak at 0.802 eV observed above $I = 17.7\mathrm{W/cm}^2$ was not identified but presumably originated from a charged exciton. Therefore, we conclude that InAsP QDs were formed on annealed InP NWs and that emission from a single QD in an NW up to the C-band was obtained.

5. Conclusions

In conclusion, we succeeded in reducing the tip size of InP nanowires by *in-situ* thermal annealing. After a series of investigations on the annealing temperature and annealing time, we found that the change in the shape of the InP NWs was caused by the thermal evaporation of P from the edge of the NW and by the diffusion of In from the sidewall to the tip, followed by the evaporation of In or the growth of InP. The optimal temperature for annealing was 600 °C in our present investigation, which was lower than the growth temperature (660 °C) for the growth of InP NWs, and NWs with a tip size of 20 nm were successfully realized. Furthermore, we confirmed the formation of InAsP QD on the annealed InP NWs, emitting in the telecom band. Our results are useful for controlling the size of NWs and for the controlled formation of InAsP NW-QDs for photonic devices suitable for telecommunication.

6. Conflicts of interest

There are no conflicts of interest to declare.

7. Acknowledgments

The authors thank Kohei Chiba, Akinori Yoshida, and Yuusuke Minami, for experimental support. This study was financially supported by KAKENHI (Grant Nos. 17H03223 and 20H02176).

Data availability statement

All data that support the findings of this study are included in the article and supplementary files.

References

[1] Tomioka K, Yoshimura M and Fukui T 2012 *Nature* **488** 189–192
[2] Barrigón E, Heurlin M, Bi Z, Monemar B and Samuelson L 2019 *Chemical Reviews* **119** 9170–9220
[3] Jia C, Lin Z, Huang Y and Duan X 2019 *Chemical Reviews* **119** 9074–9135
[4] Fukata N and Rurali R (eds) 2021 *Fundamental Properties of Semiconductor Nanowires* (Singapore: Springer Singapore)
[5] Quan L N, Kang J, Ning C Z and Yang P 2019 *Chemical Reviews* **119** 9153–9169
[6] Notomi M, Takiguchi M, Sergent S, Zhang G and Sumikura H 2020 *Optical Materials Express* **10** 2560
[7] Church S A, Al-Abri R, Parkinson P and Saxena D 2022 *Progress in Quantum Electronics* **85** 100408
[8] Dalacu D, Poole P J and Williams R L 2019 *Nanotechnology* **30** 232001
[9] Chang J, Gao J, Zadeh I E, Elshaari A W and Zwiller V 2023 *Nanophotonics* **12** 339–358
[10] Zhang G, Tateno K, Sogawa T and Gotoh H 2018 *Nanotechnology* **29** 155202
[11] Jaffal A, Regreny P, Patriarche G, Gendry M and Chauvin N 2021 *Nanoscale* **13** 16952–16958
[12] Kawaguchi K, Sudo H, Matsuda M, Ekawa M, Yamamoto T and Arakawa Y 2015 *Japanese Journal of Applied Physics* **54** 04DN02
[13] Zhang G, Gnatek D, Takiguchi M, Xu X, Tateno K, Sasaki S, Tawara T and Gotoh H 2020 *Japanese Journal of Applied Physics* **59** 105003
[14] Zhang G, Takiguchi M, Tateno K, Tawara T, Notomi M and Gotoh H 2019 *Science Advances* **5** eaat8896
[15] Loitsch B, Rudolph D, Morkötter S, Döblinger M, Grimaldi G, Hanschke L, Matich S, Parzinger E, Wurstbauer U, Abstreiter G, Finley J J and Koblmüller G 2015 *Advanced Materials* **27** 2195–2202
[16] Bulgarini G, Reimer M E, Zehender T, Hocevar M, Bakkers E P A M, Kouwenhoven L P and Zwiller V 2012 *Applied Physics Letters* **100** 121106
[17] Bulgarini G, Reimer M E, Bouwes Bavinck M, Jöns K D, Dalacu D, Poole P J, Bakkers E P A M and Zwiller V 2014 *Nano Letters* **14** 4102–4106
[18] Reimer M E, Bulgarini G, Akopian N, Hocevar M, Bavinck M B, Verheijen M A, Bakkers E P A M, Kouwenhoven L P and Zwiller V 2012 *Nature Communications* **3** 737
[19] Haffouz S, Zeuner K D, Dalacu D, Poole P J, Lapointe J, Poitras D, Mnaymneh K, Wu X, Couillard M, Korkusinski M, Schöll E, Jöns K D, Zwiller V and Williams R L 2018 *Nano Letters* **18** 3047–3052
[20] Saxena D, Mokkapati S, Parkinson P, Jiang N, Gao Q, Tan H H and Jagadish C 2013 *Nature Photonics* **7** 963–968
[21] Kunimoto T, Obara S, Hara S and Motohisa J 2023 *Japanese Journal of Applied Physics* **62** SC1072
[22] Zhang X, Yi R, Zhao B, Li C, Li L, Li Z, Zhang F, Wang N, Zhang M, Fang L, Zhao J, Chen P, Lu W, Fu L, Tan H H, Jagadish C and Gan X 2023 *ACS Nano* **17** 10918–10924
[23] Versteegh M A M, Reimer M E, Jöns K D, Dalacu D, Poole P J, Gulinatti A, Giudice A and Zwiller V 2014 *Nature Communications* **5** 5298
[24] Jöns K D, Schweickert L, Versteegh M A M, Dalacu D, Poole P J, Gulinatti A, Giudice A, Zwiller V and Reimer M E 2017 *Scientific Reports* **7** 1700–1711
[25] Gudiksen M S and Lieber C M 2000 *Journal of the American Chemical Society* **122** 8801–8802
[26] Yu H, Li J, Loomis R A, Wang L W and Buhro W E 2003 *Nature Materials* **2** 517–520
[27] Kitauchi Y, Kobayashi Y, Tomioka K, Hara S, Hiruma K, Fukui T and Motohisa J 2010 *Nano Letters* **10** 1699–1703
[28] Sekiguchi H, Kishino K and Kikuchi A 2008 *Applied Physics Express* **1** 122837–124002
[29] Gao Q, Dubrovskii V G, Caroff P, Wong-Leung J, Li L, Guo Y, Fu L, Tan H H, Jagadish C, Gua Y, Fu L, Tan H H and Jagadish C 2016 *Nano Letters* **16** 4361–4367

[30] Kohashi Y, Sakita S, Hara S and Motohisa J 2013 *Applied Physics Express* **6** 025502
[31] Dalacu D, Kam A, Guy Austing D, Wu X, Lapointe J, Aers G C and Poole P J 2009 *Nanotechnology* **20** 395602
[32] Brockway L, Pendyala C, Jasinski J, Sunkara M K and Vaddiraju S 2011 *Crystal Growth & Design* **11** 4559–4564
[33] Ilkiv I, Kirilenko D, Kotlyar K and Bouravleuv A 2020 *Nanotechnology* **31** 055701
[34] Schmiedeke P, Panciera F, Harmand J C, Travers L and Koblmüller G 2023 *Nanoscale Advances* **5** 2994–3004
[35] Del Giudice F, Becker J, De Rose C, Döblinger M, Ruhstorfer D, Suomenniemi L, Treu J, Riedl H, Finley J J and Koblmüller G 2020 *Nanoscale* **12** 21857–21868
[36] Cirlin G E, Tchernycheva M, Patriarche G and Harmand J C 2012 *Semiconductors* **46** 175–178
[37] Farrow R F 1974 *Journal of Physics D: Applied Physics* **7** 2436–2448
[38] Minot E D, Kelkensberg F, van Kouwen M, van Dam J A, Kouwenhoven L P, Zwiller V, Borgström M T, Wunnicke O, Verheijen M A and Bakkers E P A M 2007 *Nano Letters* **7** 367–371
[39] Tchernycheva M, Cirlin G E, Patriarche G, Travers L, Zwiller V, Perinetti U and Harmand J C 2007 *Nano Letters* **7** 1500–1504
[40] Zhong Z, Li X, Wu J, Li C, Xie R B, Yuan X, Niu X, Wang W, Luo X, Zhang G, Wang Z M, Tan H H and Jagadish C 2019 *Applied Physics Letters* **115** 053101
[41] Chang T Y, Kim H, Hubbard W A, Azizur-Rahman K M, Ju J J, Kim J H, Lee W J and Huffaker D 2022 *ACS Applied Materials and Interfaces* **14** 12488–12494
[42] Dalacu D, Mnaymneh K, Lapointe J, Wu X, Poole P J, Bulgarini G, Zwiller V and Reimer M E 2012 *Nano Letters* **12** 5919–5923
[43] Tatebayashi J, Ota Y, Ishida S, Nishioka M, Iwamoto S and Arakawa Y 2012 *Applied Physics Letters* **100** 263101–263104
[44] Tatebayashi J, Kako S, Ho J, Ota Y, Iwamoto S and Arakawa Y 2015 *Nature Photonics* **9** 501–505
[45] Balgarkashi A, Ramanandan S P, Tappy N, Nahra M, Kim W, Güniat L, Friedl M, Morgan N, Dede D, Leran J B, Couteau C and Fontcuberta I Morral A 2020 *Journal of Optics (United Kingdom)* **22** 084002
[46] Haffouz S, Poole P J, Jin J, Wu X, Ginet L, Mnaymneh K, Dalacu D and Williams R L 2020 *Applied Physics Letters* **117** 113102
[47] Priante G, Ambrosini S, Dubrovskii V G, Franciosi A and Rubini S 2013 *Crystal Growth and Design* **13** 3976–3984
[48] Kim W, Dubrovskii V G, Vukajlovic-Plestina J, Tütüncüoglu G, Francaviglia L, Güniat L, Potts H, Friedl M, Leran J B and Fontcuberta I Morral A 2018 *Nano Letters* **18** 49–57 ISSN 15306992
[49] Dorenbos S, Sasakura H, Van Kouwen M, Akopian N, Adachi S, Namekata N, Jo M, Motohisa J, Kobayashi Y, Tomioka K, Fukui T, Inoue S, Kumano H, Natarajan C, Hadfield R, Zijlstra T, Klapwijk T, Zwiller V and Suemune I 2010 *Applied Physics Letters* **97** 171106
[50] Sasakura H, Hermannstädter C, Dorenbos S N, Akopian N, Van Kouwen M P, Motohisa J, Kobayashi Y, Kumano H, Kondo K, Tomioka K, Fukui T, Suemune I and Zwiller V 2012 *Physical Review B* **85** 075324
[51] Yanase S, Sasakura H, Hara S and Motohisa J 2017 Single-photon emission from InAsP quantum dots embedded in density-controlled InP nanowires *Japanese Journal of Applied Physics* vol 56 p 04CP04

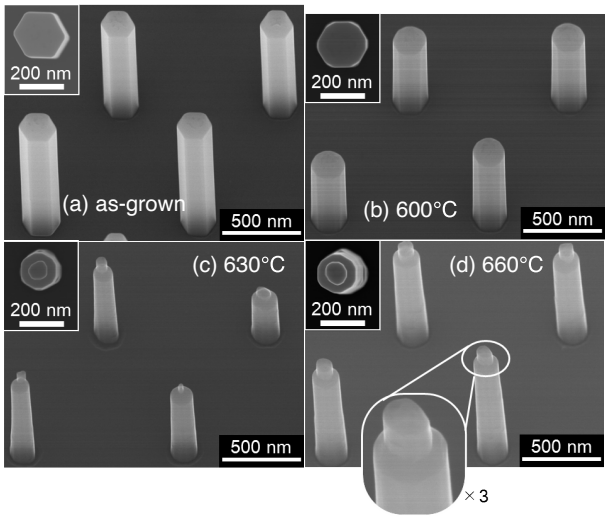

Figure 1. SEM images of InP NWs with and without annealing and their temperature dependence for NW with initial diameter d of 240 nm. (a) as-grown InP NWs, (b) annealing temperature $T_A = 600°C$, (c) $T_A = 630°C$, and (d) $T_A = 660°C$.

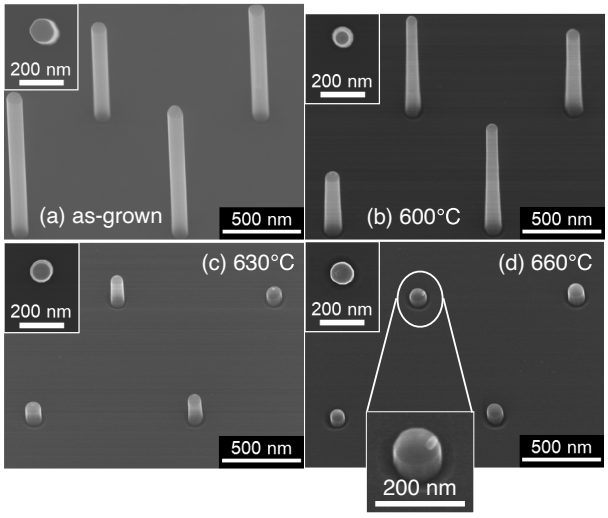

Figure 2. SEM images of InP NWs with and without annealing and their temperature dependence for NW with initial diameter d of 120 nm. (a) as-grown InP NWs. (b), (c), and (d) show the results after annealing at 600, 630, and $T_A = 660°C$, respectively.

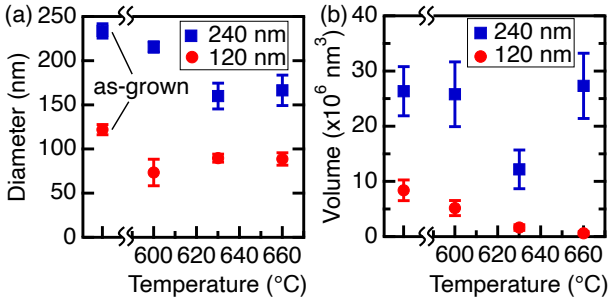

Figure 3. Change of diameter (a) and volume (b) of InP NWs induced by annealing and its temperature dependence.

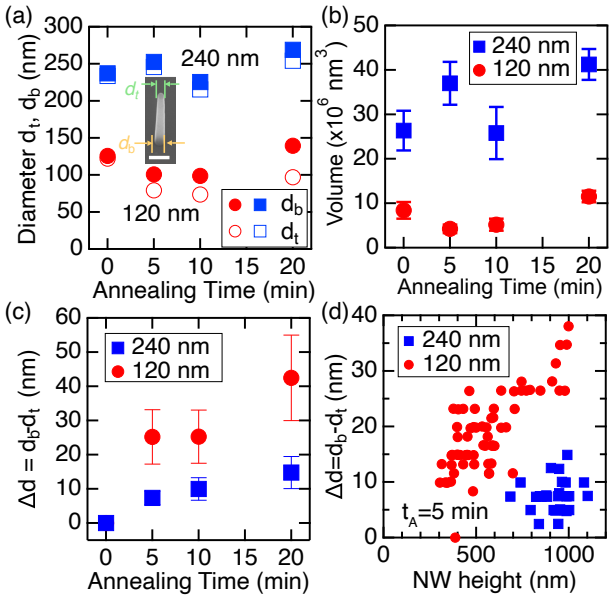

Figure 4. Dependence of the diameter (a) and volume (b) of NW on annealing time at T_A = 600°C. Inset of (a) shows an SEM image of NW annealed for 5 min with d=120 nm. Scale bar is 200 nm. (c) Evolution of the difference of the top and bottom height $\Delta d = d_t - d_b$ under annealing at T=600 °C. (d) Comparison of the top and bottom size of NWs after 5 min annealing at 600 °C for NWs with d = 120 and 240 nm.

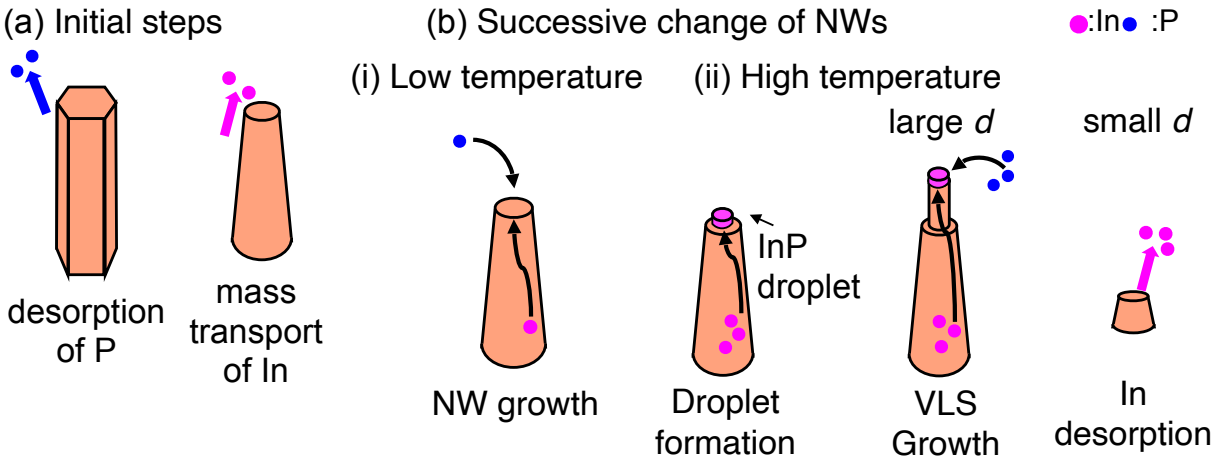

Figure 5. Model for the shape change of NW by annealing. (a) In the initial steps of annealing process, desorption of P and mass transport of In takes place. (b) Successive change of NWs during annealing is either (i) a normal epitaxial growth at low temperature or (ii) formation of In droplet and VLS growth, or desorption of In at higher temperatures. The process (ii) depends on the size of the droplet and NW diameter.

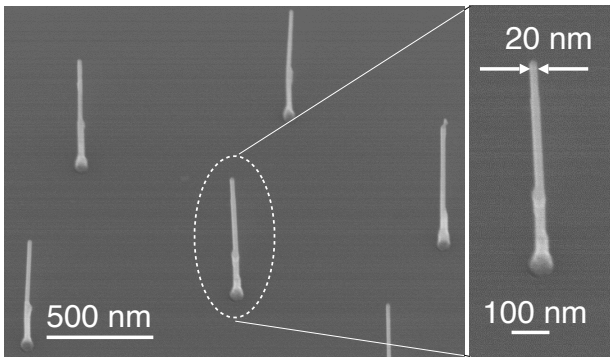

Figure 6. SEM image of NWs with a diameter of about 20 nm obtained by annealing at 600 °C for 5 min. The initial opening size d_0 of the mask was 60 nm.

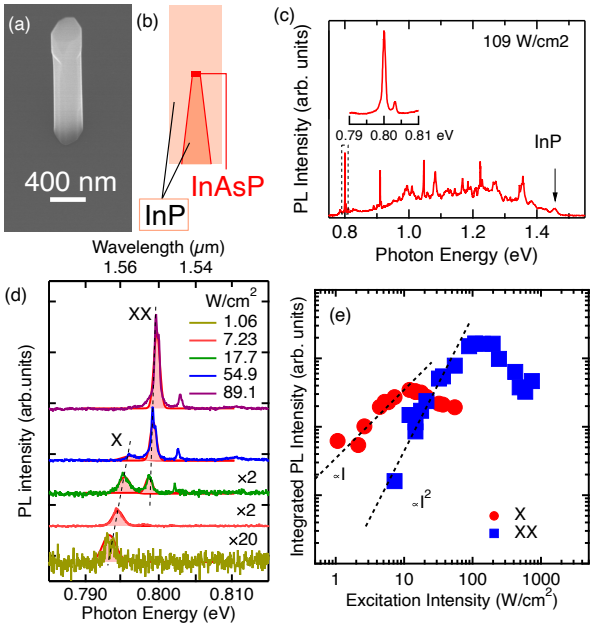

Figure 7. (a) SEM image of a single InP/InAsP/InP vertical heterostructure NW formed after the annealing of InP NW. and (b) its schematic cross-section. (c) Low-temperature PL spectra of heterostructure NW. (d) Excitation intensity dependence of the PL spectra of a single InAsP QD emission formed heterostructure NW with annealed InP NW. (e) Dependence of the integrated intensity of peak X and XX on the excitation intensity I.